Turbulent Extreme Multi-Zone Model for Multi-Waveband Variations of Blazars

A. P. Marscher
Institute for Astrophysical Research, Boston University, 725 Commonwealth Ave., Boston, MA 02215, USA

The author is developing a numerical code with thousands of emission zones to simulate the time-dependent multi-waveband emission from blazars. The code is based on a model in which turbulent plasma flowing at a relativistic speed down a jet crosses a standing conical collimation shock that accelerates electrons to maximum energies in the 5-100 GeV range. This paper reports early results produced by the model. The simulated light curves and time profiles of the degree and position angle of polarization have a number of features in common with the observational data of blazars. Maps of the polarized intensity structure can be compared with those of blazars observed with very long baseline interferometry at short millimeter wavelengths.

1. INTRODUCTION

Reproduction of the time-dependent multi-waveband emission of blazars poses severe theoretical challenges. Observations with the Very Long Baseline Array (VLBA) at 7 mm wavelength [Marscher et al. 2012] have found that the majority of γ-ray flares in blazars are simultaneous with either the passage of a new superluminal knot through the bright stationary feature termed the "core" or a brightening of the core with no prominent knot subsequently appearing. The core lies parsecs from the central engine in blazars [see Marscher 2006, for a discussion]. Nevertheless, time-scales of flux changes can be as short as hours, even for very high-energy γ rays that must also be emitted on parsec scales to avoid a high opacity to pair-production [e.g., Aleksic et al. 2011].

One way to explain the rapid variability so far from the central engine is to imagine that the emission arises from localized regions where Doppler factors exceed the values derived from apparent superluminal speeds of radio knots. Two possibilities to realize this scenario have been proposed: magnetic reconnections [Giannios et al. 2009] and relativistic turbulence [Marscher and Jorstad 2010, Narayan and Piran 2012]. The author is developing a numerical code, called the Turbulent Extreme Multi-Zone (TEMZ) model, that can compute the time-dependent spectral energy distribution (SED) and therefore multi-frequency light curve for these physical scenarios. Thus far, the code has been applied to an approximate simulation of turbulent plasma crossing a standing conical shock in the jet. It includes two sources of seed photons for inverse Compton scattering: a hot, dusty torus and a Mach disk (also often called a "working surface"), which is a strong shock oriented transverse to the jet flow that occupies a small portion of the jet cross-section centered on the axis [Courant and Friedrichs 1948]. One of the primary merits of this effort is that the simulations can be compared with the wealth of data produced by multi-waveband monitoring programs: light curves, SEDs, and polarization vs. time, frequency, and position. This progress report presents early results from this effort.

2. DESCRIPTION OF THE TEMZ MODEL

The code is based on a model in which turbulent plasma flowing at a relativistic speed down a jet crosses a standing conical collimation shock that accelerates electrons to energies up to some maximum value, probably in the range from 5 to 100 GeV. The code divides the plasma into many cells (see Fig. 1), each with a different direction of magnetic field. This provides a crude simulation of turbulence. The energy density of electrons is modulated randomly such that the variations in flux produce a power spectral density described by a power law with a slope similar to the observed value in the range of 1.2-2 [Larsson 2012]. The direction of the magnetic field is different for each cell, and the maximum electron energy generated at the shock can either depend on that direction or be set randomly within a probability distribution. The plasma in each cell has a turbulent velocity with random direction superposed on the systemic flow velocity. As the plasma flows across the shock and then loses energy as it advects downstream, variations in the synchrotron and inverse Compton flux, as well as in the linear polarization, occur over a range of time-scales. Since the standing shock lies parsecs from the central engine, radiation from a hot dust torus and a Mach disk at the vertex of the shock cone can both be significant sources of seed photons from the scattering. Emission from the latter varies along with the energy density of the plasma, although the photons from an outburst require months to diffuse across the cells; this smoothes the fluctuations of the seed photon field. Traditional synchrotron self-Compton (SSC) scattering of the synchrotron radiation emitted by each of the cells other than the Mach disk is not included in the current, non-parallelized version of the code owing to the excessive cpu time needed.

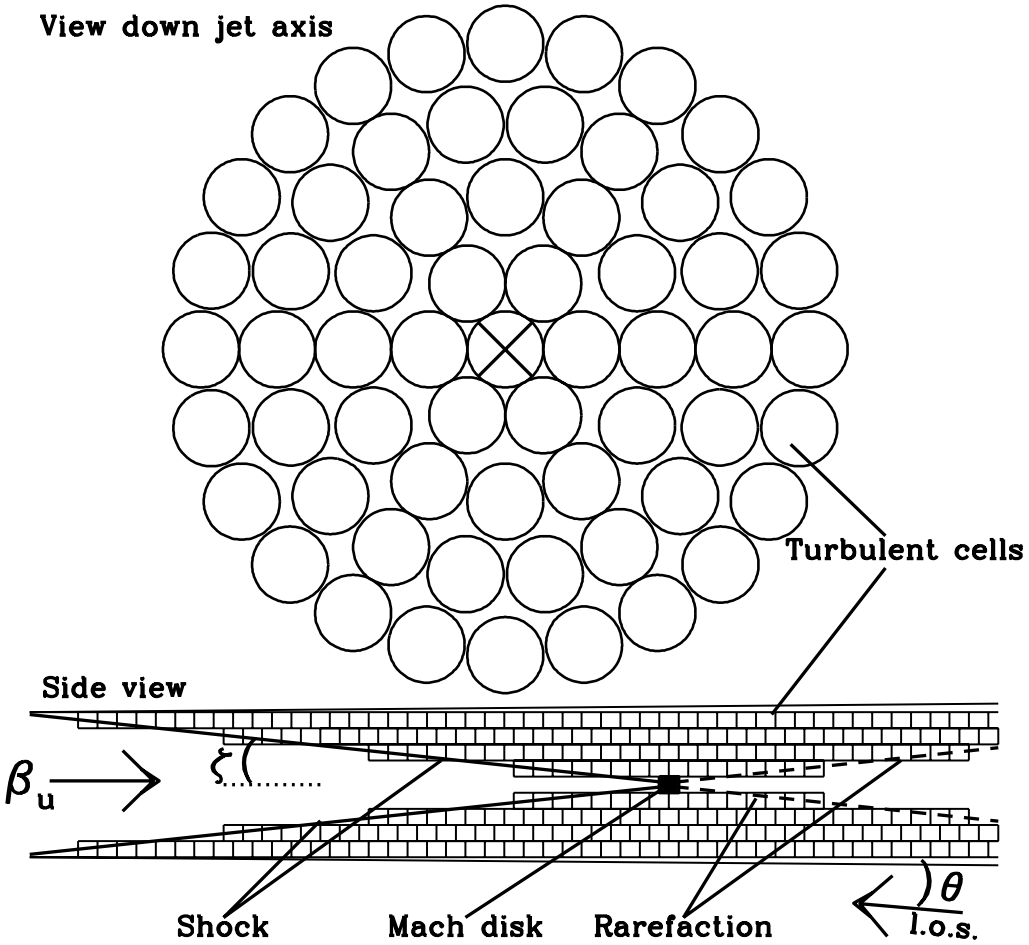

Figure 1: Schematic of the TEMZ model showing the shock, rarefaction, and cylindrical cells. The emission is assumed to occur between the conical standing shock and the rarefaction. The only practical restriction on the number of cells $N_{\rm cross}$ across the jet cross-section (as seen in view down axis on bottom) is the memory of the computer, although the mean observed degree of linear polarization $\langle \Pi_{\rm opt} \rangle$ at optical wavelengths provides a guideline: $N_{\rm cross} \sim 1.4 \langle \Pi_{\rm opt} \rangle^{-1/2}$.

The motivation for the model arises from salient observed properties of the multi-frequency behavior of blazars. Most of these properties are ignored as "weather" in other models, but are used by the author to both shape the TEMZ model and provide tests of its ability to represent the physics of blazars. The critical observations include: (1) red-noise power spectra of flux variations in blazars [e.g., Abdo et al. 2010, Chatterjee et al. 2008, 2012, Larsson 2012], (2) shorter time-scales of variability of flux and polarization at higher frequencies [Marscher 2012], (3) mean polarization levels as well as fractional deviations from the mean that are higher at optical than at lower frequencies [D'Arcangelo 2010, Jorstad et al. 2007], (4) apparent rotations in polarization position angle that are really just random walks of the projected magnetic field direction [D'Arcangelo 2010, D'Arcangelo et al. 2007], (5) breaks in the synchrotron spectrum by more than the radiative loss value of 0.5 [e.g., Wehrle et al. 2012], and (6) flares that are often sharply peaked or contain multiple peaks, neither of which is reproduced by single- or few-zoned models. The dependence of items 2-4 on frequency is directly related to the change in spectral index beyond the break, according to the model [Marscher and Jorstad 2010].

An important feature of the model is the different value of the maximum electron energy $\gamma_{0,\rm max}$ that is achieved by particle acceleration at the shock front. This can either be determined randomly from within a power-law probability distribution [Marscher and Jorstad 2010] or as a function of the angle that the magnetic field of the cell subtends to the shock normal. The simulations presented here adopt $\gamma_{0,\rm max}$ times $\cos^2(B_\parallel/B)$, where the subscript $\parallel$ indicates the

component of the magnetic field that is parallel to the shock normal. The value of $\gamma_{0,\max}$ is not allowed to fall below some minimum value, which is set as an input parameter. Future development can include results from Monte Carlo calculations of particle acceleration in relativistic shocks [e.g., Summerlin and Baring 2012].

The code currently includes synchrotron radiation, inverse Compton scattering (IC) of seed photons from a hot dust torus, and IC of synchrotron + SSC radiation from relatively slowly moving plasma in a Mach disk at the vertex of the conical shock. The last of these is abbreviated as "SSC-MD." If a Mach disk is present, this can be the dominant SSC emission, since the seed photons are Doppler boosted in the frame of the turbulent cells. The combined effects of co-spatiality of the emission regions at different wavebands, non-uniform electron energy distribution, different magnetic field orientations for different turbulent cells, and light-travel delays, cause correlations of variations at pairs of wavebands but with time lags and often a lack of one-to-one correspondence of flares. This is similar to the observed behavior of blazars [e.g., Marscher 2012, Wehrle et al. 2012]. The code generates simulations of flux (at 68 frequencies from 10^{10} to 10^{26} Hz) and polarization (at radio to optical frequencies) vs. time.

The synchrotron flux density of a cell depends on (among other factors): (1) the volume filling factor of electrons with energies high enough to radiate at the frequency of observation, (2) the spectral index α, determined by the slope of the electron energy distribution, (3) the normalization factor N_0 of the electron energy distribution, and (4) the strength B and angle ψ (corrected for relativistic aberration) of the magnetic field relative to the line of sight through the factor $(B \sin\psi)^{1+\alpha}$.

Meanwhile, the inverse Compton X-ray or γ-ray flux density depends on: (1) the volume filling factor of electrons with energies high enough to scatter the highest-frequency seed photons to the observed photon energy, (2) the slope of the electron energy distribution, (3) the normalization factor N_0 of the electron energy distribution, and (4) the energy density of seed photons, which is constant for photons emitted by a dust torus and nearly constant if from the broad emission-line region, but variable if from a relatively slow region inside the jet, such as a Mach disk.

Since some of these factors are different for the two processes and for the different sources of seed photons, there will be a correlation but not a one-to-one correspondence between light curves at two widely separated frequencies despite the electron energies being roughly the same for optical and γ-ray emission. Even for relatively closely spaced frequencies (e.g., optical and near-IR), differences in volume filling factor as a function of maximum electron energy will weaken

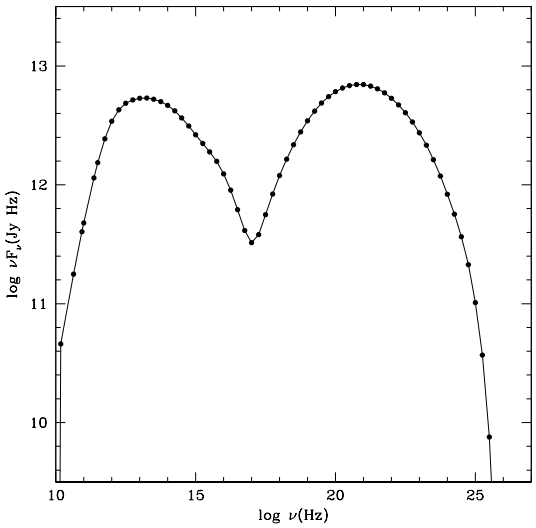

Figure 2: Sample spectral energy distribution produced by the TEMZ code, with physical parameters selected to produce emission similar to that of BL Lac during a γ-ray flare (see Fig. 5). Note the power-law shape in the near-IR, optical, and near-UV range with a spectral index of 1.3, significantly steeper than both the input lower-frequency value of $\alpha_{\rm low} = 0.55$ and the high-frequency value $\alpha_{\rm low} + 0.5 = 1.05$ that one would expect solely from radiative energy losses. This results from the combination of radiative losses and the dependence of the highest energy to which electrons are accelerated by the shock on the angle between the magnetic field and the shock front (see text).

the correlations of the light curves and polarization vs. time. At very high photon energies, "orphan flares" are possible if, e.g., the magnetic field of the cell that contains the highest energy electrons points directly along the line of sight. In this example, no synchrotron flare would be seen even during a major γ-ray flare. A Mach disk at the end of the conical recollimation shock can provide a variable source of seed photons that is well beamed in the frame of the plasma passing through the recollimation shock but not in the observer's frame, since the flow speed of the plasma beyond the Mach disk is only mildly relativistic. Temporarily bright regions in a relatively slow sheath of the jet could produce a similar effect. The code allows each cell to have a randomly oriented turbulent velocity relative to the general jet flow. This, along with the different maximum electron energy and magnetic field direction in the different cells, as well as the small volume of each cell, allows for very fast variability at optical and γ-ray frequencies [see Narayan and Piran 2012].

If one compares the results of a simulation (Fig. 3) with actual data [see Fig. 5 as well as, e.g., Wehrle et al. 2012], the results look quite promising. One can see in the plots a number of cases of apparently "orphan"

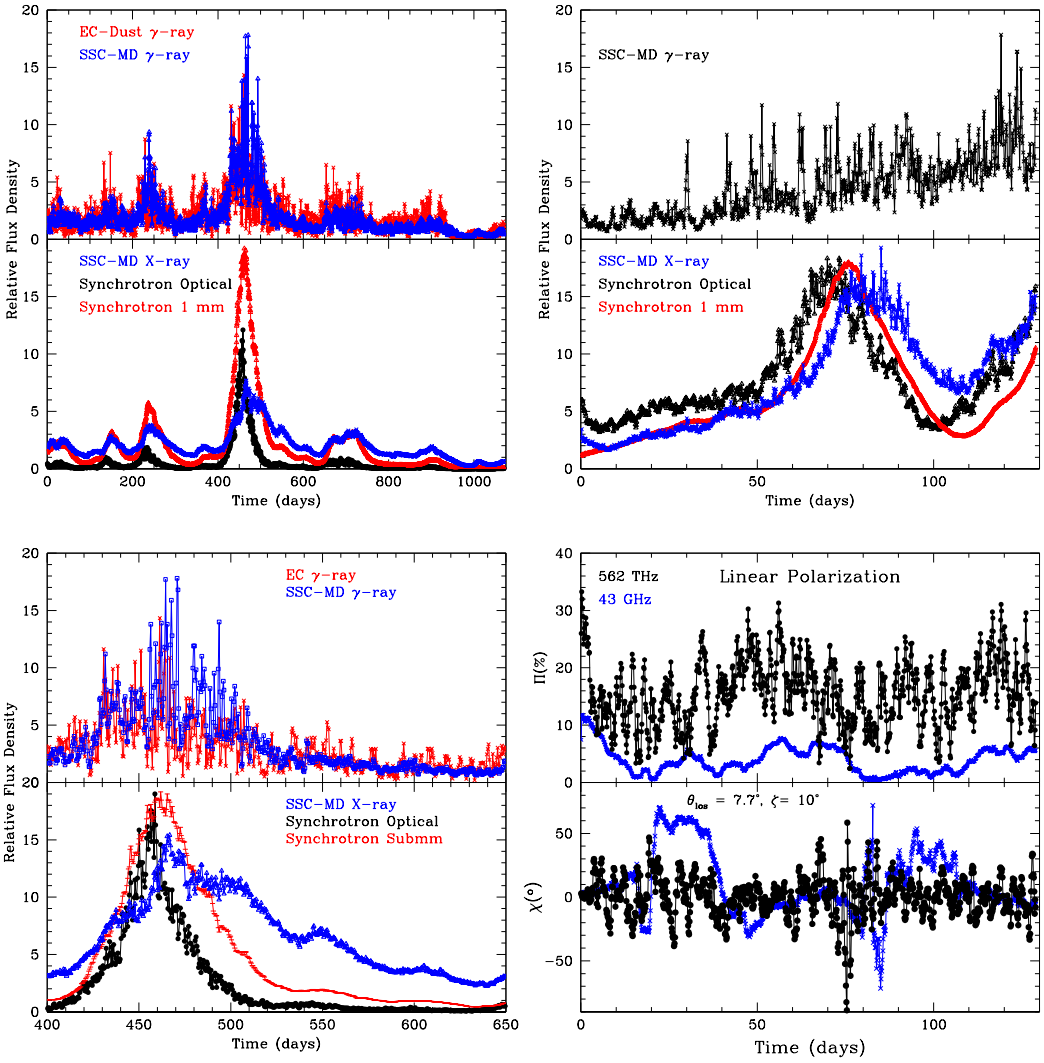

Figure 3: Sample simulated light curves and linear polarization vs. time generated by the TEMZ code. *Left:* Input parameters similar to those inferred observationally for 3C 454.3 [Wehrle et al. 2012], with $N_{\rm cross} = 60$ (see the caption of Fig. 1). Bottom panel focuses on the brightest flare seen in the top panel. *Right:* Input parameters similar to those inferred observationally for BL Lac [Marscher 2012], with $N_{\rm cross} = 126$. Note the changing ratios of high-energy to optical flux, sharply peaked flares, more rapid variations at higher frequencies (γ-ray vs. X-ray and optical vs. mm-wave), stronger linear polarization at higher frequencies (optical vs. mm-wave), apparent rotations in polarization position angle χ, and preferred polarization position angle same as jet direction (0° in the simulation). Some examples of orphan γ-ray flares are seen. All of these are observed properties of blazars.

γ-ray flares, and many flares are sharply peaked rather than rounded, although outbursts at lower frequencies are more rounded because they occur over larger volumes. Apparent rotations in the polarization vector occur in both clockwise (decreasing χ) and counterclockwise directions, as observed in some blazars [e.g. Hayashida et al. 2012].

Future development includes parallelization of a C++ version of the code (which was originally written in Fortran-77) so that it can be run efficiently on a multi-processor computer. This will allow the inclusion of SSC of time-delayed seed photons from cells other than the Mach disk, thought to be important at least in BL Lac objects, if not quasars. In addition, emission-line radiation from a cloud that lies next to the parsec-scale jet [see León-Taveres et al. 2013] will be added. This can be an additional source of time-variable seed photons, since the excitation of the cloud

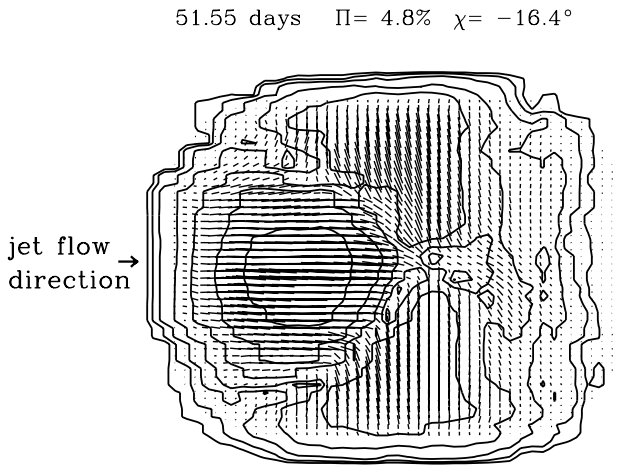

Figure 4: Sample polarized intensity map of the emission region between the standing shock and the rarefaction shown in Fig. 1, at time 51.55 days in the same simulation as the one that produced the right-hand side of Figure 3. The contours are in factors of 2 starting at 1% of the maximum in polarization intensity. The lengths of the line segments are proportional to the polarized intensity, and they are aligned with the polarization direction. The orientation is similar to that of Fig. 1, with the jet base to the left. The integrated degree Π and position angle χ of polarization are indicated, with $\chi = 0^\circ$ parallel to the jet axis (left-right in the figure) and positive values of χ counterclockwise to this direction. Note that, despite the near-cancellation of the polarization from different parts of the jet, an image of sufficiently high angular resolution would reveal strong gradients in both the degree and position angle of polarization.

will depend on the flux of UV photons emitted by the jet.

The eventual goal is to run the code over a range of input parameters to determine the physical conditions under which various observational features can be reproduced. Each simulation is a unique combination of both random and systematic processes, and so will not reproduce actual light curves. However, statistical analyses of the timing characteristics — correlations across frequencies, power spectra, and variations of polarization in both time and frequency — can be compared with the same characteristics of the data obtained from comprehensive monitoring programs such as that led by the author's group [Marscher et al. 2010]. In addition, ultra-high resolution polarized intensity images, such as those now becoming available with VLBI at a wavelength of 3 mm [Martí-Vidal et al. 2012], can verify whether the distinct polarization structure produced by turbulent plasma crossing the standing conical shock (see Fig. 4) is seen in nature.

Acknowledgments

The author gratefully acknowledges financial support for this research from NASA Fermi Guest Investigator grant NNX12AO79G and, during the earlier stages, National Science Foundation grant AST-0907893. This work benefitted from International Team collaboration 160 sponsored by the International Space Science Institute (ISSI) in Switzerland.

References

A.A. Abdo, et al., *Astrophys. J.* **722**, 520 (2010).
A. Aleksic, et al., *Astrophys. J. Lett.* **730**, L8 (2011).
T. V. Cawthorne, *MNRAS* **367**, 851 (2006).
R. Chatterjee et al., *Astrophys. J.*, **689**, 79 (2008).
R. Chatterjee et al., *Astrophys. J.*, **749**, 191 (2012).
R. Courant and D. B. Friedrichs, *Supersonic Flow and Shock Waves* (Springer-Verlag, New York, 1976).
F.D. D'Arcangelo, "Correlated Multiwavelength Polarization in Blazars," Ph.D. Thesis, Boston U. (2010).
F.D. D'Arcangelo et al., *Astrophys. J. Lett.*, **659**, L107 (2007).
D. Giannios, D. A. Uzdensky, and M. C. Begelman, *MNRAS* **395**, L29 (2009).
M. Hayashida, *Astrophys. J.*, **754**, 114 (2012).
S.G. Jorstad et al., *Astron. J.*, **134**, 799 (2007).
S. Larsson, paper presented at 2012 Fermi Symposium (2012).
J. León-Taveres et al., *Astrophys. J. Lett.*, **763**, L36 (2013).
A.P. Marscher, in Relativistic Jets: The Common Physics of AGN, Microquasars and Gamma-Ray Bursts, AIP Conf. Ser. **856**, ed. P.A. Hughes & J.N. Bregman, 1 (2006).
A.P. Marscher, in *2011 Fermi Symposium*, eConference C110509, ed. A. Morselli, arXiv:1201.5402 (2012).
A.P. Marscher *et al.*, *Astrophys. J. Lett.* **710**, L126 (2010).
A. P. Marscher, S.G. Jorstad, I. Agudo, N.R. MacDonald, & T.L. Scott, in *Proceedings of Fermi & Jansky: Our Evolving Understanding of AGN*, ed. R. Ojha, D. Thompson, & C.D. Dermer, eConference C1111101, arXiv:1204.6707 (2012).
A.P. Marscher and S.G. Jorstad, in *Fermi Meets Jansky: AGN in Radio and Gamma Rays*, ed. T. Savolainen, E. Ros, R.W. Porcas, and J.A. Zensus (Max-Planck-Institut für Radioastronomie, Bonn), p. 171, arXiv:1005.5551 (2010).

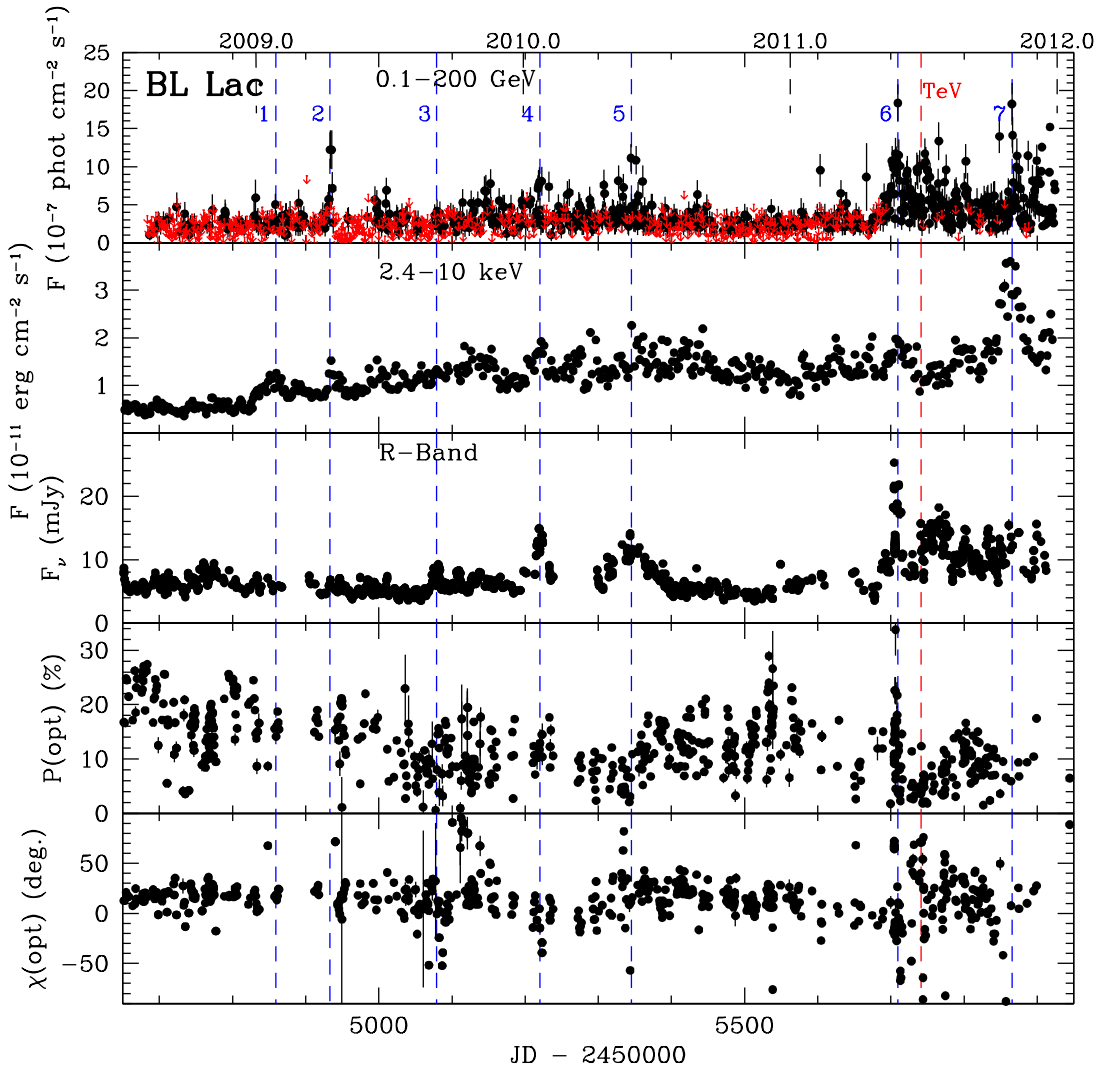

Figure 5: Multi-waveband flux and degree P and electric-vector position angle χ of optical polarization vs. time for BL Lac in 2011. Note rapid variations in P and χ, indicative of a turbulent magnetic field. Data are from Marscher et al. (in preparation).

I. Martí-Vidal et al., *Astron. Astrophys.*, **542**, A107 (2012).
R. Narayan and T. Piran, *MNRAS* **420**, 604 (2012).
E.J. Summerlin and M.G. Baring, *Astrophys. J.*, **745**, 63 (2012).
A.E. Wehrle et al., *Astrophys. J.*, **758**, 72 (2012).